

Electron momentum density in liquid siliconK. Matsuda,¹ T. Nagao,¹ Y. Kajihara,² M. Inui,² K. Tamura,³ J. Nakamura,^{1,*} K. Kimura,¹ M. Yao,¹ M. Itou,⁴ Y. Sakurai,⁴ and N. Hiraoka⁵¹Graduate School of Science, Kyoto University, Kyoto 606-8502, Japan²Graduate School of Integrated Arts and Sciences, Hiroshima University, Higashi Hiroshima 739-8521, Japan³Graduate School of Engineering, Kyoto University, Sakyo-ku, Kyoto 606-8501, Japan⁴Japan Synchrotron Radiation Research Institute, SPring-8, 1-1-1 Kouto, Sayo, Hyogo 679-5198, Japan⁵National Synchrotron Radiation Research Center, Hsinchu 30076, Taiwan

(Received 10 March 2013; published 16 September 2013)

The electron momentum density (EMD) in liquid silicon (Si) has been measured by synchrotron-based Compton scattering. The observed variation in the valence EMD upon melting, reflecting a semiconductor-metal transition of Si, is well explained by the collapse of the Jones zone of crystalline Si. However, the shape of the EMD of liquid Si is considerably broad and retains fairly solid (α -Si)-like characteristics. The analysis of the Fourier-transformed Compton profiles reveals that the valence electronic state in liquid Si exhibits a marked deviation from the free-electron gas features.

DOI: [10.1103/PhysRevB.88.115125](https://doi.org/10.1103/PhysRevB.88.115125)

PACS number(s): 71.22.+i, 71.20.Mq, 71.30.+h

I. INTRODUCTION

Elemental silicon (Si) is a typical semiconductor in the solid state. Upon melting, Si undergoes a semiconductor-metal transition. The molar volume contracts and the nearest-neighbor coordination number increases. The electrical conductivity increases by a factor of 20 and becomes about $1.3\text{--}1.4 \times 10^4 \Omega^{-1} \text{cm}^{-1}$,¹ which is comparable to those of typical liquid metals. However, liquid Si has several unique properties compared with simple liquid metals. A small shoulder has been observed in the main peak of the structure factor of liquid Si,² which is not usually observed in simple liquid metals. Moreover, the coordination number of liquid Si is 6–7, which is relatively small compared with those of simple liquid metals, 10–12.

The fact that liquid Si has a rather open structure has been prompting intensive investigations to elucidate the essential feature of such unique properties of liquid Si. *Ab initio* molecular dynamics (AIMD) simulation³ enabled the visualization of the time evolution of the charge density of valence electrons in liquid Si, and the accumulation of charge between adjacent atoms at a very short time (~ 30 fs) was observed, which was interpreted as a remnant of covalent bonds forming the local tetrahedral order. A theoretical calculation based on the pseudopotential theory also revealed that the bond-angle distribution shows a single peak close to the tetrahedral bond angle.⁴ Inelastic x-ray scattering measurements showed an additional enhancement of the atomic correlation time on the subpicosecond level, which was discussed in relation to the formation of the covalent bonds in liquid Si.⁵ Recent orbital-free AIMD simulation also revealed a short-lived charge accumulation between adjacent atoms,⁶ however, such charge accumulation was not attributed to the existence of “covalent bonds.”

Several investigations concerning the valence electronic state in liquid Si have thus far been carried out. Magnetic susceptibility measurements⁷ indicated that liquid Si is a simple metal in which the four valence electrons behave as conduction electrons. X-ray emission⁸ and photoelectron spectroscopy (PES) measurements^{9,10} revealed the appearance of density

of states (DOS) with a clear Fermi edge, demonstrating the typical metallic nature of liquid Si. The PES measurements, however, exhibit a distinct dip in the middle of the DOS, which cannot simply be described by the free-electron gas model and was interpreted as the existence of *s-p* hybridization in the liquid. Recently, inelastic x-ray Compton scattering measurements were carried out for liquid Si heated by a levitation technique, and a persistence of covalent bonding in the liquid was reported on the grounds that the experimentally obtained Compton profile (CP) difference agrees with the CP difference obtained by the Car-Parrinello molecular dynamics simulation.¹¹

Compton scattering measurements are a unique technique for measuring the momentum densities of electrons in materials.^{12,13} In this work, using a sample cell made of sapphire, which enables stable measurements for a highly volatile fluid sample even at high temperatures,¹⁴ we carried out x-ray Compton scattering measurements of liquid Si near the melting temperature and solid Si at various temperatures. In Ref. 11 the observed feature of the CP difference was attributed to the fact that the effect of covalent bond breaking is dominant over the effect of Si site disorder. Our measurements also showed variation of the valence CP of Si upon melting, and such variation can be simply explained by the collapse of the Jones zone. A more important finding of our investigation is that the shape of the EMD and the magnitude of variation upon melting are of crucial importance for characterizing the valence electronic state in liquid Si. We derived EMDs from CPs and found that the shape of the EMD of liquid Si shows a significant resemblance to that of the semiconducting solid (α -Si) state, suggesting that the valence electronic state in liquid Si retains fairly α -Si-like characteristics. Such a view is substantiated by our finding that the magnitude of the variation in the EMD upon melting is smaller than that theoretically calculated for the transformation to a denser metallic solid Si (β -Si). Furthermore, the results of analysis based on the reciprocal form factors $B(r)$ of valence electron CPs reveal that the valence electronic state in liquid Si exhibits a marked deviation from the free-electron gas features.

II. EXPERIMENT

In a Compton scattering experiment, the double differential scattering cross section is associated with the EMD $\rho(\mathbf{p})$ of the scattering system under the condition of impulse approximation¹⁵ as follows:

$$\frac{d^2\sigma}{d\Omega d\omega} \propto J(p_z) = \iint \rho(\mathbf{p}) dp_x dp_y. \quad (1)$$

Here $J(p_z)$ is the so-called Compton profile (CP), which is the projection of $\rho(\mathbf{p})$ along the photon scattering vector (z axis).

The scattering experiments were performed at BL08W/SPring-8 using the standard setup installed in the beamline for Compton scattering experiments, consisting of a Cauchois-type bent-crystal analyzer and a position-sensitive detector. The energy of the incident x rays is 115.6 keV, the energy of the scattered x rays ranges from 70 to 90 keV and the scattering angle is 165° . An x-ray image intensifier camera was used as a position-sensitive detector.¹⁶ The momentum resolution is 0.13 a.u. (atomic units) in this experiment.

Liquids at high temperatures should be contained in a cell made of a special material transparent to x rays as well as resistant to the corrosive nature of hot metallic liquids. Thus, single-crystalline sapphire was used as the material for the cell. The cell consists of two closed-end sapphire tubes with a radial thickness of 0.5 mm and different outer diameters of 6 and 5 mm. The closed end of each tube through which x rays passed was mechanically polished to be as thin as 0.25 mm. These tubes were inserted into each other and a sample space was created between them. A polycrystalline solid (α -Si) sample with a thickness of 7 mm and a diameter of 4 mm was sandwiched between these tubes. See details of the cell fabrication in Ref. 17.

High-temperature conditions were achieved with an internally resistance-heated vessel made of high-tensile steel that was specially designed for x-ray Compton scattering measurements.¹⁸ The vessel has pressure-sealed beryllium x-ray windows and enables experiments under high-pressure conditions created by He gas compression. In this study, Compton scattering measurements were carried out in He gas atmosphere rather than in vacuum because liquid Si is highly volatile. He gas was kept at a pressure of 24.2 MPa to suppress evaporation. We carried out Compton scattering measurements for liquid Si at 1773 K, which is 80 K higher than the melting point of Si (1685 K). The count rate is ~ 7 cps at the peak position, and the measurement of one scan took approximately 16 h and the total counts at the peak position reached $\sim 4.0 \times 10^5$, which is one order of magnitude larger than those in Ref. 11. We also measured the CPs of solid Si at several temperatures (298, 973, and 1573 K) to compare them with that of liquid Si. We succeeded in obtaining the Compton scattering spectra of liquid and solid Si with good statistical accuracy. Then, we carried out the measurements of an empty cell to estimate the background from the cell.

CPs were derived from the raw spectra of scattered x rays by the following procedures. First, the background was subtracted from a raw spectrum. Next, the spectrum was corrected using the efficiency of the detector. Then, the correction of the absorption of the incident and scattered x rays in the sample and that of the energy-dependent Compton

scattering cross section were carried out. Furthermore, double scattering contributions were estimated by the Monte Carlo simulation technique developed by Sakai,¹⁹ and they were subtracted from the spectrum. Finally, they were folded at zero momentum and normalized to the number of electrons per formula unit. For deriving valence-electron CPs, we assume that the core-electron profile $J_c(p)$ is well represented by the theoretical CP obtained by Hartree-Fock calculation.²⁰ The valence-electron CP $J_v(p)$ was derived by subtracting the theoretical core-electron profile from the total CP, where the iteration procedure in Ref. 13 was used under the assumption that the valence CP becomes zero above 5 a.u.

III. RESULTS AND DISCUSSION

A. Compton profiles

Figure 1(a) shows the valence-electron CPs of liquid and solid Si. Variation of the CP upon melting was certainly observed. As shown in the inset, such variation can be clearly seen when the profile of liquid Si is compared with the profiles of solid Si under all measurement conditions. The $J_v(p)$ of liquid Si has a sharper slope than that of solid Si and intersects with it at around $p \simeq 0.9$ a.u. The estimated statistical error is less than 0.3%, which is sufficiently small compared with the observed difference. These results indicate that the shape of the CP of liquid Si is narrower than that of solid Si. If only the density change were responsible for the variation in

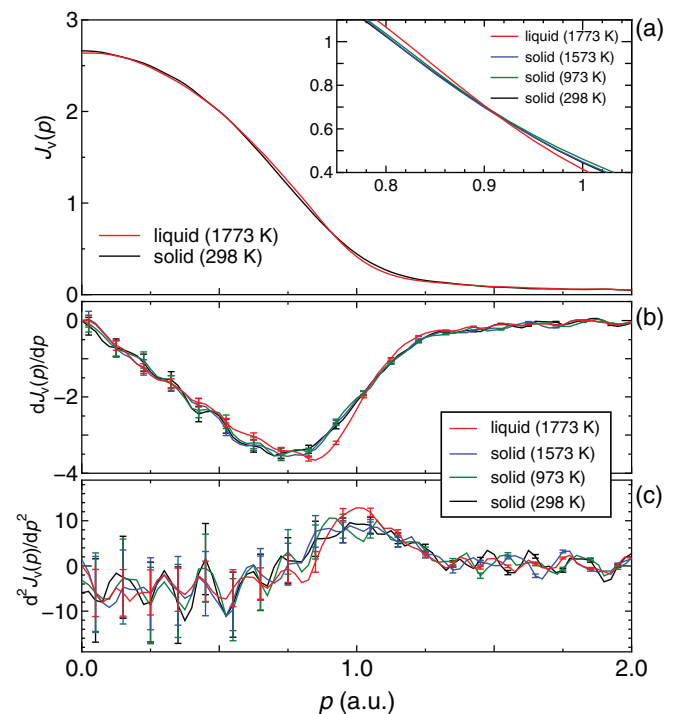


FIG. 1. (Color online) (a) Valence-electron CPs of liquid and solid Si normalized to four electrons (number of valence electrons per atom). For solid Si, only the profile at 298 K is shown in the main panel because profiles of solid Si are similar to each other irrespective of temperature (see the inset). The inset shows the enlargement of the momentum region from 0.75 to 1.05 a.u. (b) The first derivative of $J_v(p)$ and (c) the second derivative of $J_v(p)$ of Si under measurement conditions. The error bars are plotted every four data points for clarity.

the CP, the densification of Si upon melting would make the CP of liquid Si broader than that of the solid state. Thus, it is reasonable to consider that such narrowing of CPs is due to the metallization of Si upon melting because the narrower Compton profile indicates the delocalization of electrons.

The first derivative $dJ_v(p)/dp$ and the second derivative $d^2J_v(p)/dp^2$ under all measurement conditions are shown in Figs. 1(b) and 1(c), respectively. The shapes of $dJ_v(p)/dp$ and $d^2J_v(p)/dp^2$ of liquid Si are clearly different from those of solid Si. The $dJ_v(p)/dp$ of liquid Si increases more sharply than those of solid Si within the momentum range from 0.8 to 1.2 a.u. As can be seen in Fig. 1(c), the second derivatives of liquid and solid Si exhibit a peak at around 1.0 a.u. In fact, it seems that the peak width of $d^2J_v(p)/dp^2$ of liquid Si is smaller than those of solid Si, because of the sharper increase in $dJ_v(p)/dp$ observed in Fig. 1(b). For metallic systems, the peak position of the second derivative provides a measure of the Fermi momentum.²¹ The evaluation of the Fermi momentum will be described later.

Here we introduce the CP difference $\Delta J_v^{A-B}(p) = J_v^A(p) - J_v^B(p)$ between the phases A and B. CP differences between the liquid CP and the solid CP under several conditions are shown in Fig. 2. The $\Delta J_v^{\text{liq.-sol.}}(p)$ is pronounced within the momentum region from 0.6 to 1.4 a.u., in which a broad maximum and a minimum are observed at about 0.8 and 1.05 a.u., respectively. Also shown in the figure is the CP difference between solids at 298 and at 1573 K, $\Delta J_v^{\text{sol.-sol.}}(p)$. In contrast to the $\Delta J_v^{\text{liq.-sol.}}(p)$, the $\Delta J_v^{\text{sol.-sol.}}(p)$ is moderate within that region.

CP differences are useful for comparing experiment and theory.¹³ $\Delta J_v(p)$ derived from theoretical calculations are also plotted in Fig. 2. We carried out two different calculations for deriving theoretical CP differences. First, we derived a CP difference by subtracting the CP calculated with the *modified* free electron gas (MFEG) model²² from the CP calculated with the free-electron gas (FEG) model. This calculation assumes that the variation of CP is caused by the collapse of the so-called Jones zone²³ of crystalline α -Si. In the MFEG model,

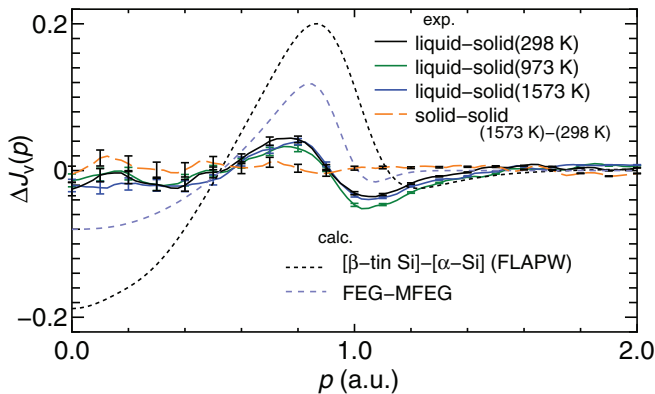


FIG. 2. (Color online) Valence electron CP differences between those under different conditions. The error bars are plotted every four data points for clarity. CP differences between MFEG and FEG and between α -Si and β -Si are also shown. The latter was calculated by the FLAPW method. For comparison with the experimental data, theoretical CPs are normalized to four electrons and broadened by the experimental resolution.

the momentum density $\rho(p)$ of crystalline Si is constructed by assuming $\rho(p)$ to be 1 and 0 inside and outside the Jones zone, respectively, neglecting the higher-order crystal potential effect.²² Then the CP of polycrystalline Si is calculated using the formula $J(p) = 2\pi \int_{|p|}^{\infty} \rho(p') p' dp'$ (Ref. 12) after the $\rho(p)$ values are directionally averaged. The normalization to four electrons is also carried out for comparison with experiment.

Second, we carried out band-structure calculations by the full-potential linearized augmented plane wave (FLAPW) method within the local-density approximation (LDA).²⁴ We calculated the valence-electron CP of polycrystalline α -Si and β -Si. The latter is a high-pressure phase of Si and is known to be metallic, thus the calculation was carried out under the assumption that its CP difference becomes a crystalline analog for the variations in the electronic properties of Si upon melting. As shown in Fig. 2, the curves of $\Delta J_v(p)$ calculated by different methods exhibit the following common features: a portion of negative values below 0.5 a.u., a positive peak at around 0.8 a.u., and a negative dip within 1.0–1.2 a.u.,. Although the $\Delta J_v^{[\beta\text{-Si}]-[\alpha\text{-Si}]}(p)$ has higher amplitude than $\Delta J_v^{\text{FEG-MFEG}}(p)$, importantly, the overall features, such as a portion of negative values in the low momentum region, a positive peak, and a negative dip, that appear in the experimental $\Delta J_v(p)$ are reproduced by the calculated $\Delta J_v(p)$. Note that both FEG and β -Si (FLAPW) CPs become narrower than their counterparts, i.e., the MFEG and α -Si (FLAPW) CPs, respectively, which supports the view that the narrowing of the experimental CP upon melting is caused by the metallization of Si.

B. Electron momentum densities

For isotropic systems, such as liquids, the EMD $\rho(p)$ can be calculated as $\rho(p) = -1/2\pi p \cdot dJ(p)/dp$.¹² Figure 3(a) shows the $\rho(p)$ of valence electrons derived from the experimental and theoretical CPs. Theoretical $\rho(p)$ were derived from the MFEG-, FEG-, and FLAPW-calculated CPs of α -Si and β -Si. In what follows, we denote them as $\rho(p)^{\text{MFEG}}$, $\rho(p)^{\text{FEG}}$, $\rho(p)^{\text{FLAPW}}_{\alpha\text{-Si}}$, and $\rho(p)^{\text{FLAPW}}_{\beta\text{-Si}}$, respectively. We also denote the experimental EMD of liquid Si and that of solid (α -) Si as $\rho_{\text{liq}}^{\text{exp}}(p)$ and $\rho_{\text{sol}}^{\text{exp}}(p)$, respectively. In the derivation of $\rho(p)$ by the above formula, valence-electron CPs were normalized to $4\pi^3 n$,¹² where n denotes the number density of valence electrons.

As shown in Fig. 3(a), the shape of $\rho_{\text{liq}}^{\text{exp}}(p)$ is considerably broader than those of $\rho^{\text{FEG}}(p)$ and $\rho_{\beta\text{-Si}}^{\text{FLAPW}}(p)$ and shows a significant resemblance to that of the semiconducting solid (α -Si) state, retaining fairly α -Si-like characteristics. Actually, it is also evident that $\rho_{\text{liq}}^{\text{exp}}(p)$ differs from $\rho_{\text{sol}}^{\text{exp}}(p)$, and $\rho_{\text{liq}}^{\text{exp}}(p)$ decreases more sharply than $\rho_{\text{sol}}^{\text{exp}}(p)$ around the momentum of ~ 0.9 a.u.

As for the EMDs of solid (α -) Si, the shape of $\rho_{\text{sol}}^{\text{exp}}(p)$ is fairly broad and exhibits a clear departure from $\rho^{\text{MFEG}}(p)$. On the other hand, the agreement between $\rho_{\text{sol}}^{\text{exp}}(p)$ and $\rho_{\alpha\text{-Si}}^{\text{FLAPW}}(p)$ is satisfactory. In fact, the characteristic features of $\rho_{\text{sol}}^{\text{exp}}(p)$ are more precisely reproduced by FLAPW calculation than by MFEG, i.e., the shape of $\rho_{\text{sol}}^{\text{exp}}(p)$ is quite broad and the values of $\rho_{\text{sol}}^{\text{exp}}(p)$ tend to be saturated at about 0.8 in the relatively low momentum region. As can be noticed from

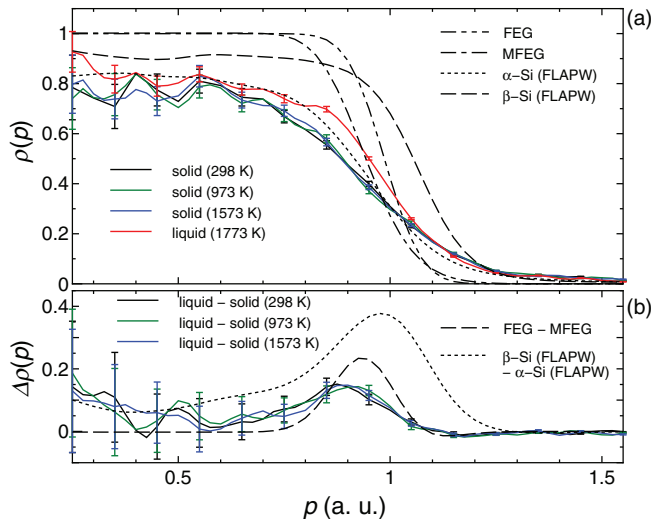


FIG. 3. (Color online) (a) Experimentally derived $\rho(p)$ of liquid and solid Si in comparison with theoretical $\rho(p)$. Theoretical $\rho(p)$ of FEG, MFEG, α -Si (FLAPW), and β -Si (FLAPW) are also shown. (b) EMD differences $\rho_{\text{liq}}^{\text{exp}}(p) - \rho_{\text{sol}}^{\text{exp}}(p)$ in comparison with calculated EMD differences $\rho_{\text{FEG}}^{\text{FLAPW}}(p) - \rho_{\text{MFEG}}^{\text{FLAPW}}(p)$ and $\rho_{\beta\text{-Si}}^{\text{FLAPW}}(p) - \rho_{\alpha\text{-Si}}^{\text{FLAPW}}(p)$. In both panels, the error bars are plotted every four data points for clarity.

the figure, exact agreement between $\rho_{\text{sol}}^{\text{exp}}(p)$ and $\rho_{\alpha\text{-Si}}^{\text{FLAPW}}(p)$ is still not achieved, which is often the case when comparing experimental and theoretical EMDs or CPs,^{25–27} however, this level of agreement is sufficient for the following discussion.

As in the case of CP differences, we also calculated EMD differences for comparison between experimental and calculated profiles. Experimental EMD differences $\Delta\rho^{\text{exp}}(p)$, which were obtained by subtracting $\rho_{\text{sol}}^{\text{exp}}(p)$ from $\rho_{\text{liq}}^{\text{exp}}(p)$, are shown in Fig. 3(b). They are plotted together with theoretical EMD differences $\rho_{\text{FEG}}^{\text{FLAPW}}(p) - \rho_{\text{MFEG}}^{\text{FLAPW}}(p)$ and $\rho_{\beta\text{-Si}}^{\text{FLAPW}}(p) - \rho_{\alpha\text{-Si}}^{\text{FLAPW}}(p)$. Both the experimental and theoretical EMD differences have peaks within the momentum range from 0.8 to 1.1 a.u. Note that the region includes the Jones-zone face, which is formed by a $\{220\}$ plane and is located at 0.866 a.u. in the momentum space. These findings indicate that the collapse of the Jones zone of solid (α -) Si is responsible for the behavior of $\Delta\rho^{\text{exp}}(p)$ within this momentum region. This can be further confirmed by the following discussion.

To compare experimental $\Delta\rho(p)$ with the theoretical one by excluding the effect due to the change in the valence electron density, it is appropriate to scale the momentum by the electron gas p_F . In the electron gas model, p_F is given by the formula $p_F = (3\pi^2 n)^{1/3}$, where n denotes the electron number density. The scaling by the electron gas p_F was also used in the comparison between directional Compton profiles to extract effectively common features among different semiconducting elements.²⁸ In this case, p_F means the Fermi momentum of the electron gas according to the corresponding valence electron density.

Figure 4 shows EMD differences plotted against the momentum scaled by the electron gas p_F . In the derivation of EMD differences, each $\rho(p)$ was first normalized to $\rho(p/p_F)$ by the p_F that corresponds to each valence electron density,

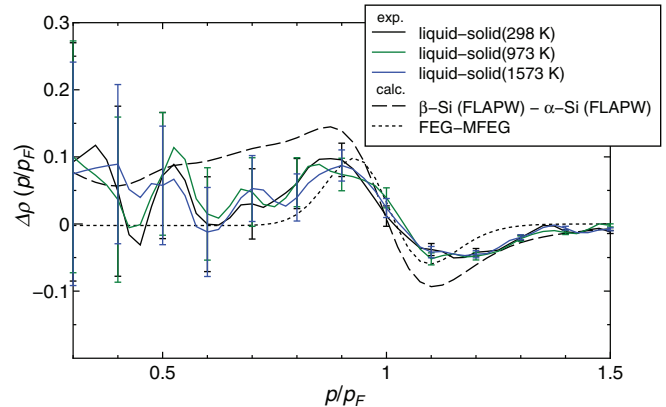


FIG. 4. (Color online) Experimental and calculated EMD differences. Prior to the subtraction among two given EMDs, the values of momentum for each EMD are normalized by the corresponding electron gas p_F . The error bars are plotted every four data points for clarity.

then the subtraction among $\rho(p/p_F)$ under different conditions was carried out.

The model for calculating $\Delta\rho(p/p_F)$ using the FEG and MFEG is quite simple, however, the overall tendency of the experimental $\Delta\rho(p/p_F)$ is well reproduced. In fact, this model (the MFEG-FEG model hereafter), which assumes that the variation of the EMD of Si can be captured by the transition from MFEG to FEG, describes the variation of the EMD due only to the collapse of the Jones-zone boundary. This is because the values of the EMD below the boundary region are kept at 1 and do not change upon transition from MFEG to FEG. Qualitative agreement between the feature of $\Delta\rho(p/p_F)$ determined using the MFEG-FEG model with that of $\Delta\rho^{\text{exp}}(p/p_F)$ indicates that the variation in the EMD of Si upon melting mainly occurs near the Jones-zone boundary. However, note that such agreement in the EMD difference does not necessarily mean that the valence electrons in liquid Si and in solid Si are well described with the FEG model and MFEG model, respectively.

As can be seen in Fig. 4, $\Delta\rho(p/p_F)$ obtained by FLAPW calculation also indicates that the shape of the EMD becomes narrow upon the transition from α -Si to β -Si, which is similar to the feature observed in the MFEG-FEG model. An important point to note is that the amplitude of $\Delta\rho(p/p_F)$ obtained by FLAPW calculation is much larger than $\Delta\rho^{\text{exp}}(p/p_F)$. The calculation predicts an appreciable increase in the EMD upon the transition from α -Si to β -Si within the range of p/p_F below ~ 1 . Actually, in this range, the experimental $\Delta\rho(p/p_F)$ has somewhat larger values than $\Delta\rho(p/p_F)$ obtained using the MFEG-FEG model. Moreover, in p/p_F regions both below ~ 0.6 and above 1.15, $\Delta\rho^{\text{exp}}(p/p_F)$ seems to approach that of FLAPW prediction. These features, the increase in momentum density in the low-momentum region and the reduction of a high-momentum tail, indicate that there exists an additional contribution in the variation of the EMD upon melting, which cannot simply be attributed to the Jones-zone boundary collapse.

An important point to note is that the amount of variation of the experimental EMD difference is considerably small compared with that expected from the α -Si to β -Si transition. It

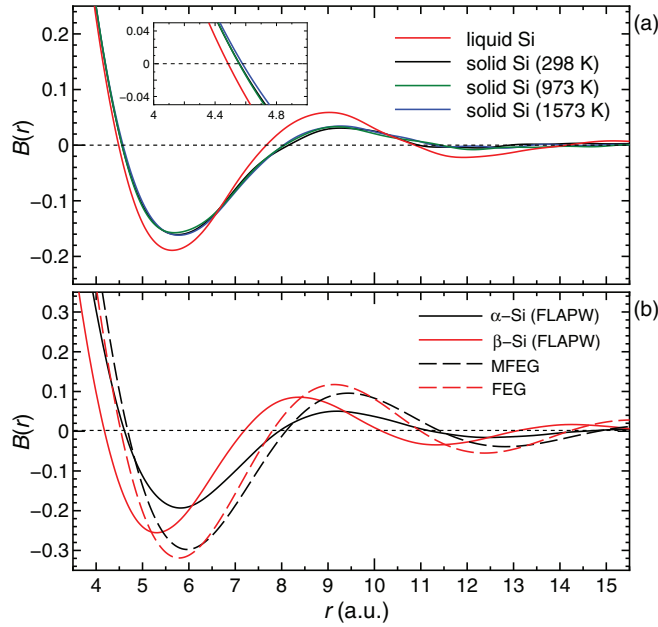


FIG. 5. (Color online) (a) Reciprocal form factors $B(r)$ of liquid and solid Si. For solid Si, the curves of $B(r)$ under three different conditions are shown. Inset shows an enlargement of the area where the curves of $B(r)$ first cross the horizontal axis (r axis). (b) $B(r)$ obtained from CPs calculated using MFEG, FEG, and FLAPW.

seems that the variation of the EMD upon melting is suppressed within the region p/p_F from 0.6 to 1.2. Considering the fact that both liquid Si and β -Si are metallic, the discrepancy between $\Delta\rho^{\text{exp}}(p/p_F)$ and $\Delta\rho(p/p_F)$ determined by the FLAPW method might originate from the different “degrees of metallization” between liquid Si and β -Si.

C. Reciprocal form factors and second derivative of CPs

For characterizing the metallic nature of liquid Si further, the position-space representation of the CPs is also of crucial importance. Figure 5(a) shows reciprocal form factors $B(r)$ obtained by the one-dimensional Fourier transformation of the experimental CPs. $B(r)$ is equivalent to the autocorrelation of the position space wave function.^{12,13} Here we calculated $B(r)$ using the formula $B(r) = \int J_v(p)e^{ipr} dp$. The range of integration was from -5 to 5 a.u. As shown in the figure, the shape of $B(r)$ of liquid Si is clearly different from those of solid Si. On the other hand, the shapes of $B(r)$ of solid Si are similar to each other. This indicates $B(r)$ is also a sensitive measure for distinguishing metallic liquid Si from semiconducting solid Si. Figure 5(b) shows MFEG-, FEG-, and FLAPW-calculated $B(r)$ of α -Si and β -Si. Essential features of the variation in $B(r)$ from α -Si to β -Si and from MFEG to FEG are similar to the variation in experimental $B(r)$ from α -Si to liquid Si, that is, the amplitude of the oscillation increases and the positions of both the first minimum and maximum shift to lower r . The increase in the oscillation amplitude is consistent with the theoretical observation²⁹ that the oscillations of $B(r)$ for metallic systems become stronger than for the corresponding insulators, indicating the enhancement of the position space correlation among electrons upon metallization.²⁹

$B(r)$ provides valuable information on the characteristic physical parameters in materials.^{12,13,29} In general, for insulators or semiconductors, the zero passages of $B(r)$ are related to the interatomic separations, whereas the zero passages of a metallic system are related to the Fermi momentum. $B(r)$ has an advantage in extracting physical information as it does not suffer from the effects of resolution broadening, multiple scattering contributions, or the ambiguities due to the core subtraction.³⁰

In this work, for semiconducting solid (α -) Si, the value of the first zero passage r_0 of the experimental $B(r)$ is 4.56 a.u. and that obtained by FLAPW calculation is 4.61 a.u. These values are close to each other but slightly above the equilibrium nearest interatomic separation of crystalline solid Si (=4.44 a.u.), which is consistent with the previously reported results for crystalline Si and Se.^{31,32}

For metallic systems, it has been regarded that r_0 is closely connected with the Fermi momentum, which can be derived by the formula $p_F = 4.493/r_0$.^{12,30} The relation is based on the analytic formula of the Fourier transformation of the free-electron gas CP, which is given as follows if the CP has unit area:

$$B(r) = \frac{3}{p_F^2 r^2} \left[\frac{\sin(p_F r)}{p_F r} - \cos(p_F r) \right]. \quad (2)$$

The zero passages of $B(r)$ are located at $p_F r = 4.493, 7.725, \dots$ and they are directly related to the Fermi momentum.^{12,30}

The lower panel of Fig. 6 shows the values of $4.493/r_0$ plotted versus $(3\pi^2 n)^{1/3}$, i.e., the electron gas p_F . Essentially, the assignment of these values to the Fermi momentum is validated when Si is in the metallic state. In fact, the value of $4.493/r_0$ is in good agreement with $(3\pi^2 n)^{1/3}$ for β -Si, indicating a fairly free-electron nature of β -Si. However, we also plotted the values of $4.493/r_0$ for semiconducting α -Si for the following discussion. As shown in the figure, the values disagree with each other for α -Si, which can be ascribed to the fact that α -Si is semiconducting and the shape of its CP is not represented by a free-electron parabola.

For liquid Si, it should be noted that the value of $4.493/r_0$ is 1.00 a.u., which is slightly larger than that of the electron gas p_F , as in the case of α -Si. Considering the fact that the shape of the EMD of liquid Si retains solid like characteristics, it is reasonable to consider that such a discrepancy is also due to non-free-electron-like (nonparabolic) contribution in the shape of the CP of liquid Si. This can also be understood from the upper panel in Fig. 6, in which Pearson’s correlation coefficients are plotted. The correlation coefficients were derived from the least square fitting of CPs by quadratic polynomial within the range $|p| \leq p_F$. As shown in the figure, there is the trend that the correlation coefficients of both α -Si and liquid Si exhibit relatively small values compared with that of β -Si.

As previously mentioned, Fermi momentum can also be estimated from the peak of the second derivative $d^2 J(p)/dp^2$ of a CP.²¹ We plotted the values of $d^2 J(p)/dp^2$ of liquid Si, α -Si, and β -Si in the lower panel of Fig. 6. As shown in the panel, the p_F value of liquid Si extracted using $d^2 J(p)/dp^2$ also exhibits a value higher than that of the electron gas p_F ,

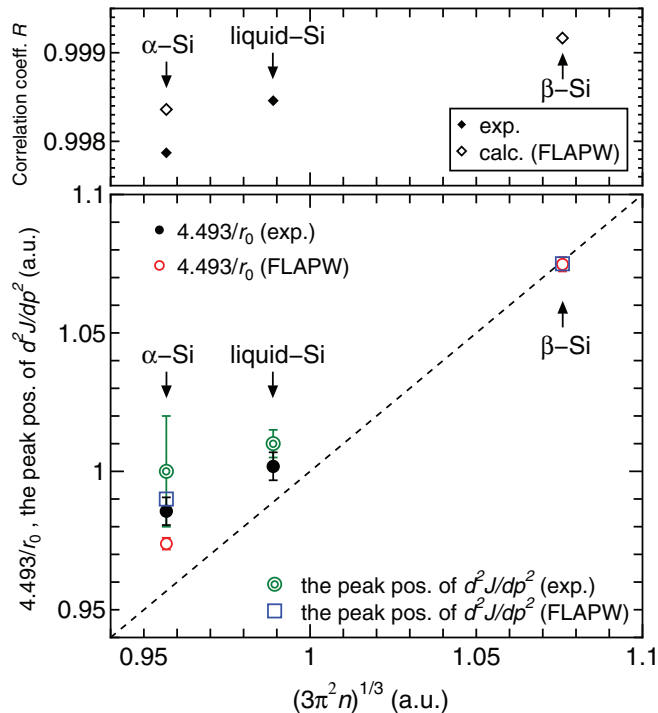


FIG. 6. (Color online) Lower panel: The values of $4.493/r_0$ [r_0 is the first zero of $B(r)$] and the peak positions of the second derivative derived for experimental CPs (α -Si at 298 K and liquid-Si) and theoretical CPs (FLAPW-calculated α -Si and β -Si) plotted versus the electron gas p_F . The short-dashed line denotes where both the values become equal. Upper panel: Pearson's correlation coefficients derived from the least square fitting of CPs by quadratic polynomial within the range $|p| \leq p_F$.

which is consistent with the feature observed for the value of $4.493/r_0$.

We also carried out the analysis of deriving Fermi momentum from CPs calculated using MFEG and FEG models and found that for each model the value of $4.493/r_0$ and the peak position of $d^2J(p)/dp^2$ are almost equal to those of corresponding electron gas p_F . The agreement found for FEG is straightforward because the shape of the CP is essentially parabolic. Also, for the MFEG model, the agreement can also be ascribed to the parabolic shape of the constructed CP (the correlation coefficient is 0.9994). This is because the model assumes the EMD to be 1 inside the Jones zone and 0 outside it, thus its shape is almost steplike, similar to that of FEG shown in Fig. 3(a). An important point to note is that FLAPW calculation, which reproduces the shape of the EMD of α -Si more precisely than does MFEG calculation, predicts the discrepancy between the value of $4.493/r_0$ and the electron gas p_F , which is consistent with the experimental trend observed for α -Si.

D. On the relation with the DOS

As for the characteristics of the valence electronic state in liquid Si, the charge accumulation between adjacent atoms forming tetrahedral order was revealed by the contour of the charge density of valence electrons visualized in the AIMD simulation, and was attributed to the remnants of covalent

bonding in liquid Si.³ Also, it has been regarded that the density of states (DOS) of the valence electrons in liquid Si does not resemble the free-electron DOS. Actually, there are some portions that cannot be described with the free-electron parabola. A distinct dip below the Fermi level was observed in the DOS measured by PES.^{9,10} Also in the theoretically calculated DOS, a step or broad peaks below the Fermi level were observed.^{4,33} These features are considered to indicate that the s state remains almost unchanged while the p state shifts to a lower binding energy upon melting, and as a result, the separation of the s and p states in the DOS of Si persists even in the liquid state.^{4,9,10,33}

We estimated the corresponding momentum range from the energy range where the distinct dip in the DOS was observed in the PES measurements. The estimated momentum range is from 0.6 to 0.9 a.u. It should be noted that, within this range, the variation of the EMD upon melting is small compared with that upon the α -Si to β -Si transition calculated using the FLAPW method. These findings suggest that the existence of such an inert portion in the variation of the EMD is closely associated with the separation of the s and p states in the DOS of liquid Si.

On the other hand, such separation of the s and p states in the DOS is less pronounced in high-pressure metallic crystals than in the metallic liquid.⁴ These observations are consistent with our finding that the value of $4.493/r_0$ and that of the electron gas p_F are slightly different for liquid Si, whereas they agree with each other for β -Si.

IV. CONCLUSION

We have measured synchrotron-based Compton scattering of solid and liquid Si with high statistical accuracy. The shape of the EMD of metallic liquid Si retains fairly solidlike features and the magnitude of the variation of EMD seems to be suppressed compared with the theoretical one calculated for the α -Si to β -Si transition; the latter is a high-pressure metallic phase of Si. Our analysis reveals that the CP features of liquid Si deviate more significantly from the free-electron features than those of β -Si, which indicates that the inhomogeneity of the valence charge distribution is more pronounced in the metallic liquid state than in the metallic solid phase.

Furthermore, the analysis of the reciprocal form factor $B(r)$ also reveals the solid(α -Si)-like nature of liquid Si through the meaningful discrepancy between the p_F derived from the first zero of $B(r)$ ($=4.493/r_0$) and the electron gas p_F , which demonstrates that these parameters reflect the shape of CPs and can be a measure for evaluating "degree of the metallic nature" of liquid Si.

Recently, it has been reported that CPs are sensitive to geometrical parameters (bond angle and length) in molecular liquid such as water and/or ice,^{34,35} demonstrating that CPs are quite effective in determining the local structures. Such analysis has not been carried out in this work for metallic liquid Si, however, considering the fact that the bond-angle distribution in liquid Si shows a single peak close to the tetrahedral bond angle,^{3,4} the observed characteristics of the EMD of liquid Si indicate the existence of such local structural fluctuation in liquid Si.

ACKNOWLEDGMENTS

The authors thank Dr. S. Ohmura for valuable discussion. This work was supported by a Grant-in-Aid for Scientific Research Fund (Research No. 19204040) and the Global COE Program “The Next Generation of Physics, Spun from Universality and Emergence” from the Ministry of Education,

Culture, Sports, Science and Technology (MEXT) of Japan. The synchrotron radiation experiments were performed at SPring-8 with the approval of the Japan Synchrotron Radiation Research Institute (JASRI) (Prop. No. 2006B1155, No. 2007A1170, No. 2008B1106, No. 2009A1252, and No. 2010B1170).

-
- *Present address: Institute of Materials Structure Science, KEK, Tsukuba, Ibaraki 305-0801, Japan.
- ¹V. M. Glazov, S. N. Chizhevskaya, and N. N. Glagoleva, *Liquid Semiconductors* (Plenum, New York, 1969).
- ²Y. Waseda and K. Suzuki, *Z. Phys. B* **20**, 339 (1975).
- ³I. Štich, R. Car, and M. Parrinello, *Phys. Rev. Lett.* **63**, 2240 (1989); *Phys. Rev. B* **44**, 4262 (1991).
- ⁴W. Jank and J. Hafner, *Phys. Rev. B* **41**, 1497 (1990).
- ⁵S. Hosokawa, W.-C. Pilgrim, Y. Kawakita, K. Ohshima, S. Takeda, D. Ishikawa, S. Tsutsui, Y. Tanaka, and A. Q. R. Baron, *J. Phys. Condens.: Matter* **15**, L623 (2003).
- ⁶L. E. González, D. J. González, and M. J. Stott, *Phys. Rev. B* **77**, 014207 (2008).
- ⁷M. Müller, H. Beck, and H.-J. Güntherodt, *Phys. Rev. Lett.* **41**, 983 (1978).
- ⁸C. F. Hague, C. S  n  maud, and H. Ostrowiecki, *J. Phys. F: Metal Phys.* **10**, L267 (1980).
- ⁹G. Gantner, H. G. Boyen, and P. Oelhafen, *Europhys. Lett.* **31**, 163 (1995).
- ¹⁰G. Gantner, H.-G. Boyen, and P. Oelhafen, *J. Non-Cryst. Solids* **205**, 490 (1996).
- ¹¹J. T. Okada, P. H.-L. Sit, Y. Watanabe, Y. J. Wang, B. Barbiellini, T. Ishikawa, M. Itou, Y. Sakurai, A. Bansil, R. Ishikawa, M. Hamaishi, T. Masaki, P.-F. Paradis, K. Kimura, T. Ishikawa, and S. Nanao, *Phys. Rev. Lett.* **108**, 067402 (2012).
- ¹²M. J. Cooper, P. E. Mijnders, N. Shiotani, N. Sakai, and A. Bansil, Eds., *X-ray Compton Scattering* (Oxford University Press, Oxford, 2004).
- ¹³W. Sch  lke, *Electron Dynamics by Inelastic X-ray Scattering* (Oxford University Press, Oxford, 2007).
- ¹⁴K. Tamura and M. Inui, *J. Phys.: Condens. Matter* **13**, R337 (2001).
- ¹⁵P. Eisenberger and P. M. Platzman, *Phys. Rev. A* **2**, 415 (1970).
- ¹⁶M. Itou, N. Hiraoka, T. Ohata, M. Mizumaki, A. Deb, Y. Sakurai, and N. Sakai, *Nucl. Instrum. Methods A* **467–468**, 1109 (2001).
- ¹⁷K. Tamura, M. Inui, and S. Hosokawa, *Rev. Sci. Instrum.* **70**, 144 (1999).
- ¹⁸K. Matsuda, K. Tamura, M. Inui, Y. Kajihara, T. Nagao, M. Yao, M. Itou, and Y. Sakurai, *Eur. Phys. J. Special Topics* **196**, 95 (2011).
- ¹⁹N. Sakai, *J. Phys. Soc. Jpn.* **56**, 2477 (1987).
- ²⁰F. Biggs, L. B. Mendelsohn, and J. B. Mann, *At. Nucl. Data Tables* **16**, 201 (1975).
- ²¹Y. Sakurai, Y. Tanaka, A. Bansil, S. Kaprzyk, A. T. Stewart, Y. Nagashima, T. Hyodo, S. Nanao, H. Kawata, and N. Shiotani, *Phys. Rev. Lett.* **74**, 2252 (1995).
- ²²W. Sch  lke, *Phys. Status Solidi B* **62**, 453 (1974).
- ²³N. F. Mott and H. Jones, *The Theory of the Properties of Metals and Alloys* (Clarendon, Oxford, 1936).
- ²⁴The code BANDS01 was supplied by Mizuho Information & Research Institute, Inc.
- ²⁵Y. Kubo, Y. Sakurai, Y. Tanaka, T. Nakamura, H. Kawata, and N. Shiotani, *J. Phys. Soc. Jpn.* **66**, 2777 (1997).
- ²⁶B. Kr  lik, P. Delaney, and S. G. Louie, *Phys. Rev. Lett.* **80**, 4253 (1998).
- ²⁷T. Ohata, M. Itou, I. Matsumoto, Y. Sakurai, H. Kawata, N. Shiotani, S. Kaprzyk, P. E. Mijnders, and A. Bansil, *Phys. Rev. B* **62**, 16528 (2000).
- ²⁸W. A. Reed and P. Eisenberger, *Phys. Rev. B* **6**, 4596 (1972).
- ²⁹P. Krusius, H. Isom  ki, and B. Kramer, *Phys. Rev. B* **19**, 1818 (1979).
- ³⁰P. Pattison and B. Williams, *Solid State Commun.* **20**, 585 (1976).
- ³¹W. Sch  lke, *Phys. Status Solidi (b)* **82**, 229 (1977).
- ³²B. Kramer, P. Krusius, W. Schr  der, and W. Sch  lke, *Phys. Rev. Lett.* **38**, 1227 (1977).
- ³³J. R. Chelikowsky and N. Binggeli, *Solid State Commun.* **88**, 381 (1993).
- ³⁴M. Hakala, K. Nyg  rd, S. Manninen, L. G. M. Pettersson, and K. H  m  l  inen, *Phys. Rev. B* **73**, 035432 (2006).
- ³⁵K. Nyg  rd, M. Hakala, S. Manninen, A. Andrejczuk, M. Itou, Y. Sakurai, L. G. M. Pettersson, and K. H  m  l  inen, *Phys. Rev. E* **74**, 031503 (2006).